Journal of Solid State Electrochemistry (2022) 26:761–772
https://doi.org/10.1007/s10008-022-05120-2

ORIGINAL PAPER

Synthesis, electrochemistry, and electrocatalytic activity of thiazole-substituted phthalocyanine complexes

Faruk Demir[1] · H. Yasemin Yenilmez[1] · Atıf Koca[2] · Zehra Altuntaş Bayır[1]

Received: 18 October 2021 / Revised: 17 December 2021 / Accepted: 12 January 2022 / Published online: 27 January 2022

Abstract

We report the synthesis of non-peripheral metallophthalocyanines which carry four 4-(4-methoxyphenyl)-2-thiazole-2-thio units. ^{1}H-NMR, FT-IR, UV–Vis, and MS data were acquired to characterize the synthesized compounds. Voltammetric and in situ spectroelectrochemical measurements shed light on the redox properties of the metallophthalocyanines (MPcs) in order to show the influence of the metal cations and thiazole-bearing substituents. In solution, the redox processes had an influence to the electrochromic responses, which were examined with in situ spectrocolorimetry. Phthalocyanines having cobalt (II), manganese (III), iron (III), and zinc (II) at the center yielded characteristic redox couples which are metal- and/or Pc-based and which are harmonious with the common redox properties of these types of compounds. In situ spectroelectrochemistry provided the information that MPc species underwent distinct color changes during electron transfer reactions. Electropolymerization of all complexes was performed on glassy carbon electrode, and the electropolymerized film of FePc was evaluated as an active electrocatalyst, in the alkaline medium, for oxygen evolution reaction (OER).

Keywords Phthalocyanine · Thiazole · Electrochemistry · Spectroelectrochemistry · Oxygen evolution reaction (OER)

Introduction

Phthalocyanines comprise of a class of molecules that are closely associated with porphyrins, having the capacity to allow various metal ions at the macrocyclic cavity, which is due to their high planarity and 18 π-electron conjugation, yielding an aromatic structure [1]. Four isoindole units are present in these porphyrin analogs and their synthesis is mainly through cyclotetramerization of phthalonitrile, diiminoisoindole, phthalic anhydride, and phthalimide. Phthalocyanines could either be peripheral or non-peripheral, depending on the starting material used, having the substituent at 4 or 3 position on the precursor, respectively.

Extensive electron-transfer abilities of the metal-bearing Pcs can be considered to be an indicator of their applications in innovative emerging fields, where the redox properties can be utilized depending upon the substituents at the periphery and the metal ion at the center [1–3].

The Q-band appearance around 600–750 nm is of rather high intensity when compared to the Soret band which appears at 300–400 nm. Moreover, one changes the substituents at the periphery along with the central metal ion, and this combination can even yield absorptions at more than 1000 nm [4].

When compared with porphyrins, phthalocyanines have higher chemical and thermal stability, improved near-IR absorption, and higher quantum yield values, and this makes MPcs perfect for manufacturing advanced aggregates of donor–acceptor feature [5].

It is of utmost importance to take the climatic and environmental issues into account, faced by the world, to search for clean-burning fuels. Water-splitting process is employed to obtain oxygen and hydrogen from water and they are light- or electricity-driven; so far, they are the most proficient methods. The splitting reaction is consisted of anodic oxygen evolution reaction (OER) and cathodic hydrogen evolution reaction (HER). OER is a slower process and it hinders the efficiency of water-splitting; however, it has a critical role in producing energy alternatives that are clean and sustainable. Fruitful results with OER are possible to develop some

✉ Zehra Altuntaş Bayır
bayir@itu.edu.tr

[1] Department of Chemistry, Faculty of Science and Letters, Istanbul Technical University, 34469 Maslak, Istanbul, Turkey

[2] Department of Chemical Engineering, Engineering Faculty, Marmara University, 34722 Göztepe, Istanbul, Turkey

power catalysts, which will boost the reaction, but this has been a challenge. MPcs have been found to serve this purpose, owing to their extraordinary properties, high availability, and low price. Substitution with various metal ions showing high catalytic activity toward OER and also being capable of bonding to –OH and O_2 helps tailor the catalytic activity of MPcs [6]. MPc complexes like CoPc, MnPc, and FePc are redox-active and they have been reported to contain more electron transfer ability because of the reduction or oxidation of metal centers than redox-inactive MPcs having Pc-based redox activities only [7–9]. The redox activity of the metal centers has the influence to technological applications, such as electrochromic materials [10], electrocatalysts in OER [11], HER [12], light absorbents in solar cells as dye sensitizers [13], and photodynamic cancer therapy [14]. For instance, Aralekallu, S. et al. studied the electrocatalytic activity of cobalt phthalocyanine containing structure as an efficient electrocatalyst for oxygen evolution reaction and reported overpotential of 370 mV at the current density of 10 mA cm − 2 with cobalt phthalocyanine polymer-coated Ni foam and overpotential of 304 mV with the mixing of cobalt phthalocyanine polymer with the benchmark catalyst IrO_2 [15]. In another study, Liao, Z. et al. reported 1.60 V onset potential with the Ni–Fe-based bimetal-phthalocyanine for the oxygen reduction reaction [16]. There are many studies in the literature on the electrocatalytic activity of MPcs, especially CoPc and FePc due to their coordination with molecular oxygen after the M(II)/M(III) oxidation of the metal centers [17–20]. It is well documented in these studies that, electrode modification methods have significant influence on the catalytic activity in addition to the nature of the catalysts. Thus, here we aimed to prepare modified electrodes with electropolymerization technique. For this purpose, we synthesized new metallophthalocyanines-bearing electropolymerizable thiazole moieties. The studies on the synthesis and electrochemistry of MPcs-bearing thiazole groups are in scare and incorporation redox-active substituents to the Pc are still taking attention to increase the redox richness of similar complexes [21–26]. Thus, here synthesis, electrochemistry and spectroelectrochemistry of thiazole-substituted phthalocyanines were examined in detail to illustrate the influence of the thiazole substituents and metal cations and to determine their possible usage in different electrochemical technologies.

In this study, we investigated the influence of thiazole groups at the periphery and metal ions at the center on the redox activity/inactivity of cobalt (II), manganese (III), iron (III), and zinc (II) phthalocyanines. Existing literature on the synthesis and electrochemistry of MPcs-bearing thiazole groups is scarce and incorporation of redox-active substituents to the periphery still attracts attention to increase the redox richness of similar complexes [21–26]. Thus, we here examined in detail the synthesis, electrochemistry, and spectroelectrochemistry of thiazole-substituted phthalocyanines to show the influence of the thiazole substituents and metal cations. In electrochemical fields, phthalocyanines required preparation of the modified electrodes for efficient use, and electropolymerization of MPcs on the electrode surface is one of the best electrode coating techniques. This is because this method allows more control on the modification process. Thus, MPcs that contain thiazole substituents, which are electropolymerizable, were employed in this study to show how the electrode is modified with electropolymerization. We tested the electropolymerization of FePc on glassy carbon electrode and used the modified electrode as a catalyst for OER.

Results and discussion

Synthesis and characterization

Electrochemical studies of thiazole groups have been reported in some publications [25, 26]. We first looked at the effect of metal ion in the macrocyclic cavity on phthalocyanines featuring electrocatalytic activity and we started the synthesis of thiazole-containing phthalocyanines. 3-nitrophthalonitrile was used as the starting material to the phthalocyanine precursor. In Scheme 1, the synthesis of dinitrile compound and the target phthalocyanines are depicted (**2**–**5**). The compound 3-[4-(4-methoxyphenyl)-2-thiazole-2-thio]-phthalonitrile (**1**) was synthesized in the reaction between 3-nitrophthalonitrile and 4-(4-methoxyphenyl)thiazole-2-thiol in N,N-dimethylformamide. The reaction was maintained at 85 °C for 24 h. In 2-dimethylaminoethanol as solvent, and metal salts ($CoCl_2$, $MnCl_2$, $Fe(CH_3COO)_2$, $Zn(CH_3COO)_2$), cyclotetramerization of compound **1** yielded the respective metallophthalocyanines (**2**–**5**). Elemental analysis and spectral data (MALDI-TOF, ^{1}H NMR, UV–Vis, and FT-IR) were employed for the elucidation of the structures.

FT-IR spectrum of compound **1** showed absorption signals at 2227 and 3112 cm^{-1}, which are assigned to C≡N and C–H stretching of the aromatic rings, respectively. The ^{1}H-NMR spectrum of **1** in DMSO-d_6 showed the signals at 3.32 ppm as singlet due to protons of CH_3 moiety. A singlet was due to the aromatic proton of the thiazole moiety at δ = 8.18 ppm. The dinitrile's aromatic protons were observed at δ = 8.10, δ = 8.05–8.03 and δ = 7.95–7.94 ppm. Doublets were spotted originating from the aromatic protons of phenoxy ring at δ = 7.83–7.81 and δ = 6.99–6.95 ppm.

In the IR spectra of phthalocyanine derivatives (**2**–**5**), the metal at the center did not make a difference. Aromatic CH and aliphatic CH vibrations were observed in the range of 3106–3055 and 2972–2829 cm^{-1}, respectively. In the ^{1}H NMR spectrum of **5**, the aromatic protons were observed

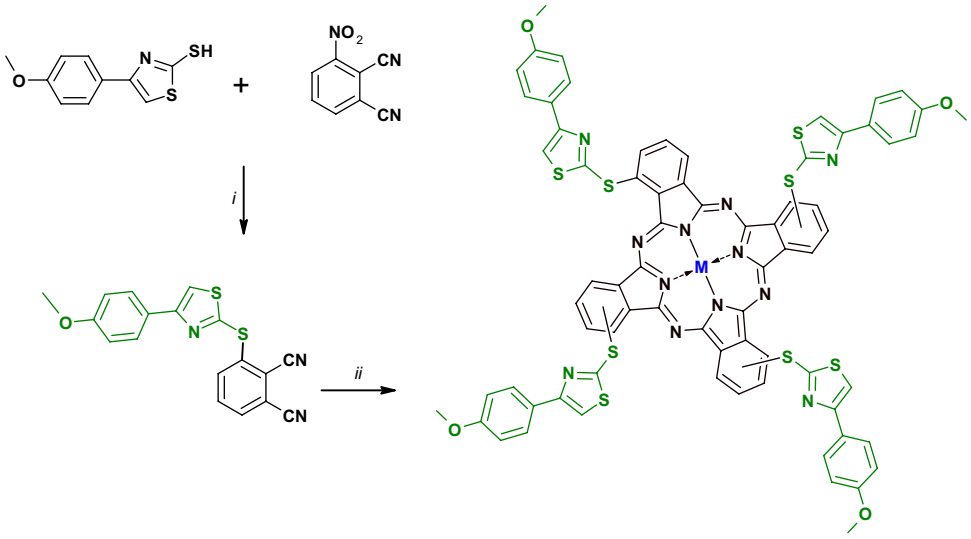

Scheme 1. Synthesis of **1**–**5**. i. K_2CO_3, DMF, 85 °C, 24 h, ii. anhydrous metal salts, 2-dimethylaminoethanol, 24 h, 135 °C (M: Co, MnCl, Fe(OAc), Zn)

between δ 8.20 and 7.01 ppm, integrating for 32 protons. Methoxy group protons were present at δ = 3.79 ppm. In the mass spectra, for FePc, $[M\text{-}Ac]^+$ ion peak was recorded at m/z = 1453.32, while $[M\text{-}Cl]^+$ ion peak for MnPc was observed at m/z = 1451.72. CoPc yielded the characteristic molecular ion peak at *m/z* = 1456.37 $[M]^+$, confirming the target structure.

The π–π* transitions in the Pc ring appear as two bands in the UV–Vis region: the Q-band in 600–700 nm region and the B-band in 300–350 nm region [27–29]. In the spectral spectrum of the heteroaromatic 18-π-electron system, π–π* transitions are seen as Q and B bands. In 1973, π → π* transition-based classification of MPc complexes was proposed by Schaeffer et al. [30, 31]. With this method, π → π* transitions are named Q, B, N, L, and C in order of increasing energy from 660 to 210 nm. If Q and B bands are present in the UV–Vis spectrum, it means that the phthalocyanine ring is formed. UV–Vis spectrum of the compounds **2, 4** and **5** in THF display typical B-bands at 327, 304, and 398 nm, and Q bands at 682, 692, and 697 nm, respectively (Fig. 1). In the UV–Vis spectrum of MnPc (**3**), the B and Q bands were observed at 349 and 749 nm, respectively. Furthermore, MnPc (**3**) shows an absorption, owing to a charge transfer as LMCT, at 505 nm [32]. It is known that the Q-bands of Mn(III)Pc derivatives appear at longer wavelengths compared to the + II oxidation states Pc metal complexes [33, 34]. As a result, 40–50 nm visible redshift is observed in the absorption spectra for Mn (III) compounds.

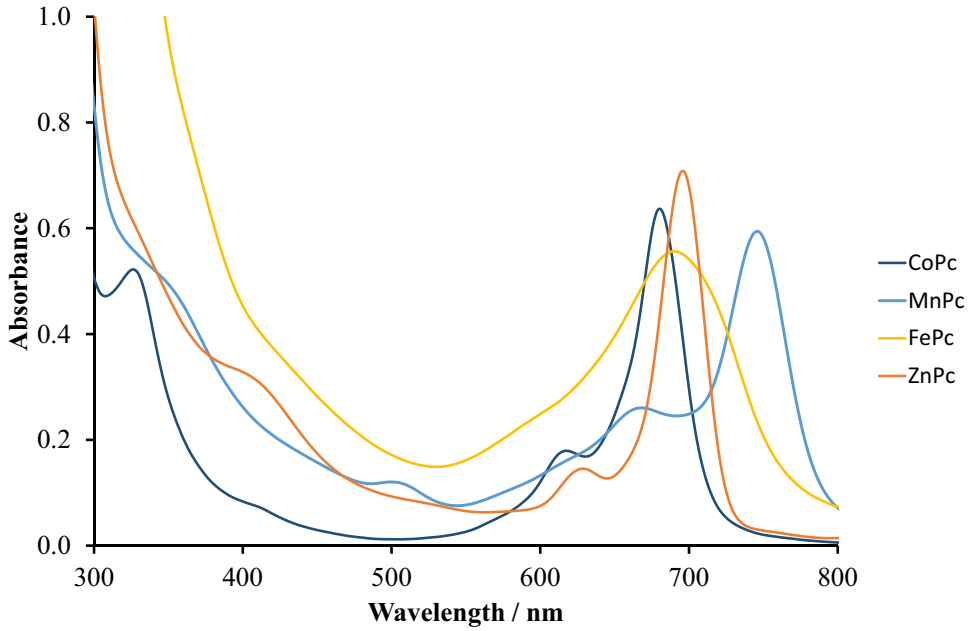

Fig. 1 UV–Vis spectrum of **2**–**5** (6×10^{-6} M in THF)

Voltammetric and spectroelectrochemical measurements

As thiazole groups are polymerizable, they are a preference in electropolymerization studies. Our group published a number of thiazole-substituted phthalocyanine compounds [13, 14, 21, 27] and by Değirmencioğlu et al. [35], but only one of them was subjected to polymerization. We prepared, in this study, new phthalocyanines carrying four 4-(4-methoxyphenyl)-2-thiazole-2-thio moieties and studied their electropolymerization properties in detail. The MPcs prepared were subjected to cyclic voltammetry and square wave voltammetry to study their electrochemical and spectroelectrochemical behaviors as to how the molecules respond to the electrochemical applications [36–39].

Table 1 lists the basic parameters, which include half-peak potential ($E_{1/2}$), anodic–cathodic peak potential separation (ΔE_p), anodic–cathodic peak current ratio (I_{pa}/I_{pc}) and the difference between the first oxidation and the first reduction potentials ($\Delta E_{1/2}$) used in the CV and SWV scans.

$\Delta E_{1/2}$ and $E_{1/2}$ values lead to the highest occupied molecular orbital (HOMO) and the lowest unoccupied molecular orbital (LUMO) energy levels and band gap. According to the reports, if the MPcs contain redox-inactive metal centers and the $\Delta E_{1/2}$ values are observed within 1.7–1.9 eV, the HOMO–LUMO transitions fall in *ca.* 650–700 nm. These MPcs are, in general, dark blue and are redox-inactive [40]. Dye sensitizers for solar cells generally employ these types of MPcs [41]. Generally, $\Delta E_{1/2}$ values less than 1.40 eV indicate that the respective MPcs are redox-active and could be employed as electrocatalysts in a wide number of applications [42]. The MPcs in this study in which the central metal is redox-active were investigated with electrochemical and spectroelectrochemical methods to shed light on their rather wide applications. The effect of Co^{2+}, Mn^{3+}, and Fe^{3+} cations at the macrocyclic center and the presence of thiazole moieties on the redox responses of the respective phthalocyanines was determined, and the results were compared with each other. The redox-active nature of these MPcs, metal-based along with the ring-based electron transfers is clearly observed.

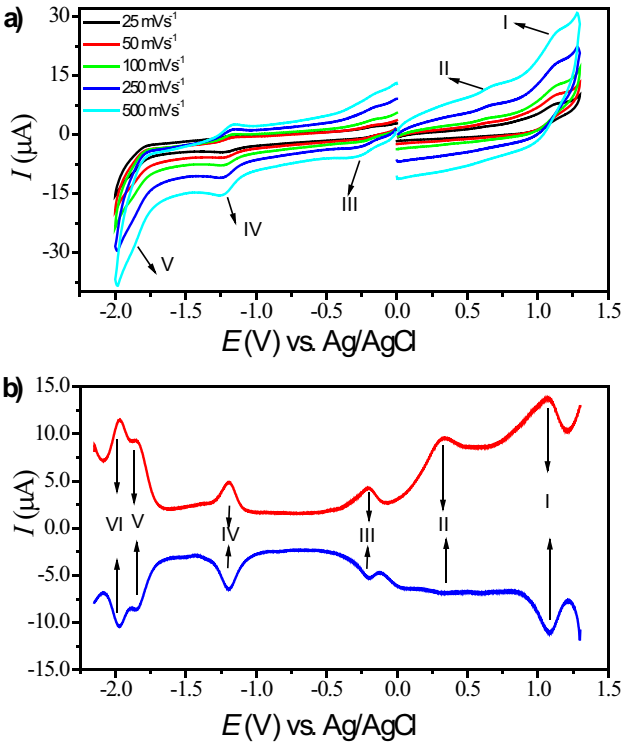

Fig. 2 **a)** CVs of CoPc (5.0×10^{-4} mol.dm^{-3}) recorded from 25 to 500 mV/s scan rates and **b)** SWV of CoPc recorded at 0.100 Vs^{-1} scan rate on a GCE working electrode in TBAP/DMF electrolyte system

In Fig. 2, CV and SWV voltammograms of CoPc on GCE in TBAP/DMF electrolyte are seen. The electrochemical behavior of CoPc yielded two oxidation waves, II at 0.61 V ($\Delta E_p = 126$ mV and $I_{p,a}/I_{p,c} = 0.80$), I at 1.04 V ($\Delta E_p = 160$ mV and $I_{p,a}/I_{p,c} = 0.79$), along with three reduction waves, III at -0.20 V ($\Delta E_p = 63$ mV and $I_{p,a}/I_{p,c} = 0.83$), IV at -1.20 V ($\Delta E_p = 58$ mV and $I_{p,a}/I_{p,c} = 0.70$), and V at -1.82 V ($\Delta E_p = 73$ mV and $I_{p,a}/I_{p,c} = 0.72$). ΔE_p, $I_{p,a}/I_{p,c}$ and peak current versus the square root of scan rates ($I_p \alpha \nu^{1/2}$) led to the conclusion that I and II oxidation waves are electrochemically and chemically quasi-reversible, and III, IV, and V reduction waves are electrochemically and chemically reversible. Metal-based reduction characters of the first

Table 1 Voltammetric data of the complexes. All data were given versus Ag/AgCl in DMF/TBAP electrolyte

Complexes	Parameters	I	II	III	IV	V	V'
CoPc	[a]$E_{1/2}$ (V)	1.04	0.61	-0.20	-1.20	-1.75	-1.82
	[b]ΔE_p (mV)	160	126	63	55	-	73
	[c]$I_{p,a}/I_{p,c}$	0.79	0.80	0.83	0.70	-	0.72
MnPc	[a]$E_{1/2}$ (V)	0.96	0.38	0.06	-0.67	-1.24	-1.74
	[b]ΔE_p (mV)	60	81	72	121	60	110
	[c]$I_{p,a}/I_{p,c}$	0.88	1.00	1.00	0.78	0.70	0.70
FePc	[a]$E_{1/2}$ (V)	1.16	0.54	0.22	-0.54	-1.04	-1.85
	[b]ΔE_p (mV)	80	60	97	60	80	90
	[c]$I_{p,a}/I_{p,c}$	1.00	0.60	1.00	0.98	0.87	1.00

reduction (III) and first oxidation (II) waves of the complex are supported by the $\Delta E_{1/2}$ and $E_{1/2}$ values (0.81 V). Slight differences between the cathodic peak currents of the III and IV processes may be due to the succeeding fast chemical reaction. This chemical reaction may be due to the coordination or non-coordination of the coordinating DMF on the central cobalt cation of the complex. Analyses of these couples indicated that the IV couple has diffusion-controlled mass transfer processes and behaves electrochemically and chemically reversible. Moreover, the possible chemical reaction succeeding the III couple slightly influences the behaviors of the IV process. 0.81 V of $\Delta E_{1/2}$ and -020 V of $E_{1/2}$ values of the III and 0.61 V of II redox couples of CoPc complex support the metal-based reduction and oxidation characters of the corresponding couple. Electrochemical measurements are solely not enough to determine the reaction mechanism of complexes. Spectroelectrochemical measurements are performed in tandem to reveal the reaction mechanisms. In situ spectroelectrochemical measurements are performed during electrolysis of the complexes

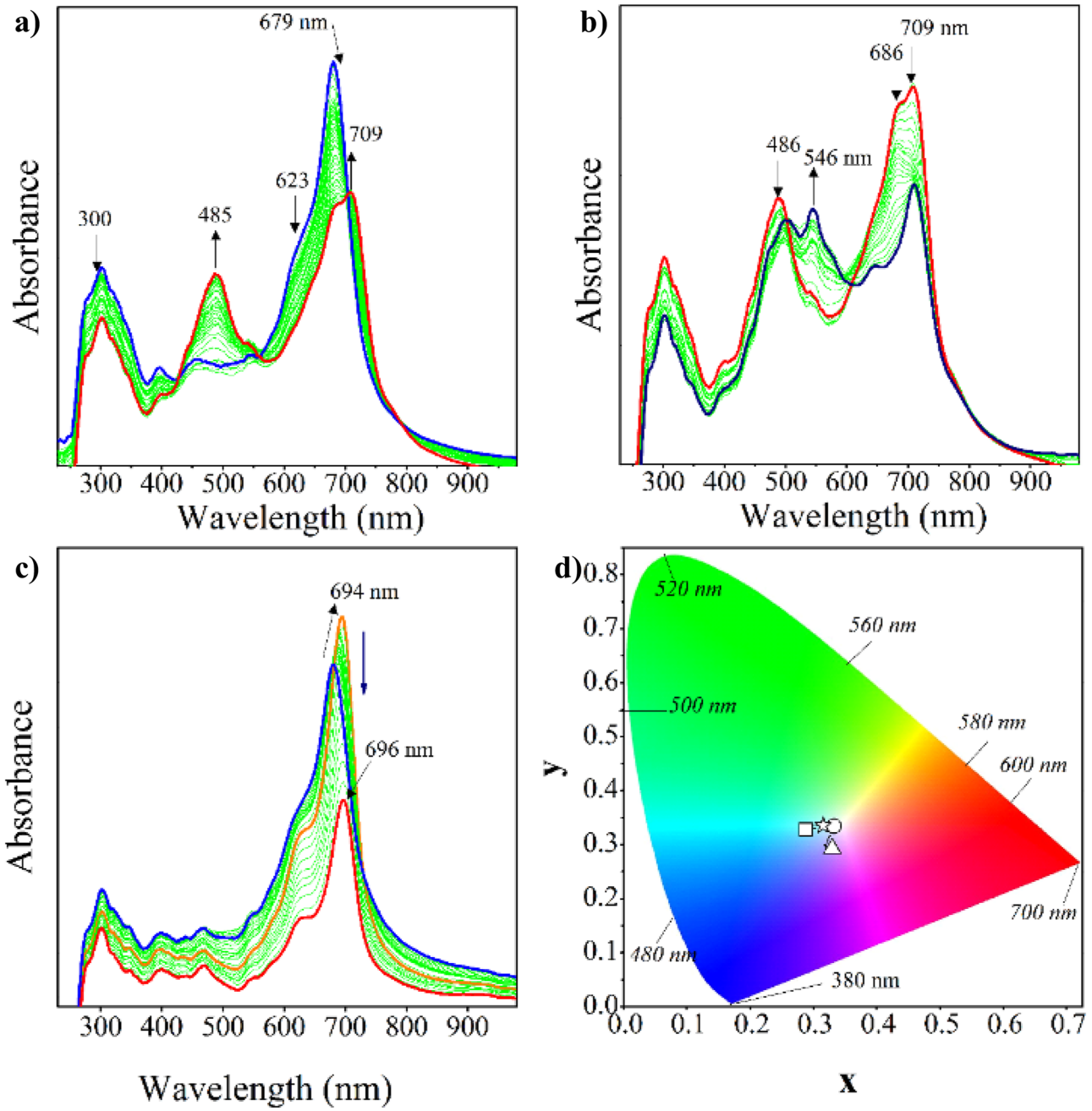

Fig. 3 In situ UV–Vis spectral changes of CoPc in TBAP/DMF electrolyte system. **a)** E_{app} = -0.40 V **b)** E_{appi} = -1.40 V **c)** E_{app} = 1.20 V, **d)** Chromaticity diagram (each symbol represents the color of electro-generated species; □: $[Co^{II}Pc^{-2}]$; O: $[Co^{I}Pc^{-2}]^{1-}$; Δ: $[Co^{I}Pc^{-3}]^{2-}$; ☆: $[Co^{III}Pc^{-2}]^{1+}$

and they help us determine the exact mechanism of the redox couples and they support the Pc and metal center electron transfer processes. Voltammetric results proposed some information about the mechanisms and spectroelectrochemical measurements clarify them. In TBAP/DMF electrolyte, CoPc's in situ UV–Vis spectrum and chromaticity responses are presented in Fig. 3.

When the first reduction potential was applied to the working electrode, the Q band at 679 nm along with a small shoulder at 623 nm undergoes hypochromism with a bathochromic shift of 30 nm and a new band was seen in the LMCT region (Fig. 3a). $[Co^{II}Pc^{-2}]/[Co^{I}Pc^{-2}]^{1-}$ process is therefore deduced owing to the couple III of CoPc (Fig. 2) [43, 44]. At -1.40 V applied potential, the spectrum in Fig. 3b is typical for a reduction in Pc. During the second reduction in the molecule, the 709 nm band decreased without shift, and a new band was observed at 546 nm. This is a clear explanation for $[Co^{I}Pc^{-2}]^{1-}/[Co^{I}Pc^{-3}]^{2}$ reduction process [45–47]. Because the Q band shifted bathochromically (Fig. 3c), the first oxidation process (II) seems to be logical for the assignment of $[Co^{II}Pc^{-2}]/[Co^{III}Pc^{-2}]^{1+}$ oxidation process. The oxidation of Pc ring is eminent as the Q band at 694 nm decreased in intensity when more positive potential was applied, and thus, second oxidation wave (I) corresponds to $[Co^{III}Pc^{-2}]^{1+}$ /$[Co^{III}Pc^{-1}]^{2+}$ process. During redox process, the color of CoPc changes and this is illustrated in Fig. 3d. CoPc's color changed from light blue (x = 0.288 and y = 0.328) to cyan (x = 0.332 and y = 0.334) during the first reduction process III. Process IV, namely the second reduction, caused the complex to go to purple (x = 0.329 and y = 0.292). In the first oxidation, the color changes from light blue (x = 0.288 and y = 0.328) to light green (x = 0.316 and y = 0.336).

The influence of Cl^{-} Mn^{III} ion at the center on the MPc system was investigated for different redox activities. Figure 4 shows that MnPc undergoes two oxidation (I and II) steps and four reductions (III, IV, V, and VI) in TBAP/DMF. Table 1 provides an analysis for these peaks and it seems that only IV and VI couples are quasi-reversible, while the other processes are electrochemically reversible. Figure 4 indicates that very low potentials, such as 0.06 and -0.67 V, are required to reduce the MnPc macrocycle as in $[Cl^{1-}\text{-}Mn^{III}Pc^{-2}]/[Cl^{1-}\text{-}Mn^{II}Pc^{-2}]^{1-}$ and the reductions following are $[Cl^{1-}\text{-}Mn^{II}Pc^{-2}]^{1-}$ to $[Mn^{II}Pc^{-2}]^{0}$) and $[Mn^{II}Pc^{-2}]/[Mn^{I}Pc^{-2}]^{1-}$ Process IV, as mentioned before, has a quasi-reversible character, and this chemical reaction might be the reason for this. Successive ring reductions for MnPc are observed as ($[Mn^{I}Pc^{-2}]^{1-}/[Mn^{I}Pc^{-3}]^{2-}$ and $[Mn^{I}Pc^{-3}]^{2-}/[Mn^{I}Pc^{-4}]^{3-}$) and these are harmonious with the literature [25, 48]. In situ spectroelectrochemistry confirms all these assignments (Fig. 5).

The UV–Vis response of MnPc during its electrolysis is shown in Fig. 5. In Fig. 5a, controlled potential

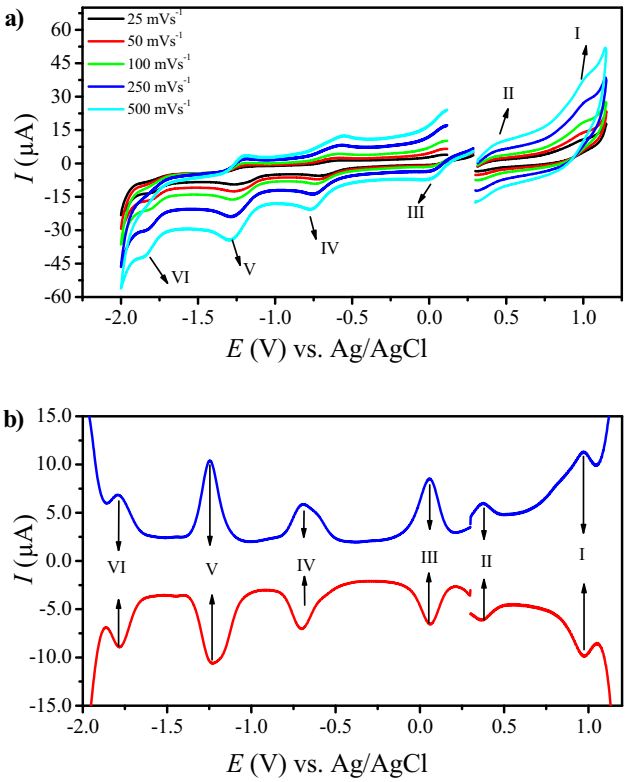

Fig. 4 **a)** CVs of MnPc (5.0×10^{-4} mol.dm^{-3}) recorded from 25 to 500 mV/s scan rates and **b)** SWV of MnPc recorded at 0.100 Vs^{-1} scan rate on a GCE working electrode in TBAP/DMF electrolyte system

reduction in MnPc at -0.40 V vs Ag/AgCl is shown, and this reduction wave corresponds to the redox potential of couple III. A hypsochromic shift from 748 to 680 nm was encountered, and new bands at 510, 581, and 854 nm were observed during this process. Metal-based reduction [49] and formation of $[Cl^{1-}\text{-}Mn^{II}Pc^{-2}]^{1-}$ species are consistent with these spectral changes. When this process was completed, $[Cl^{1-}\text{-}Mn^{II}Pc^{-2}]^{1-}$ species underwent a release of the axially bound chloride ion and a new species, namely $[Mn^{II}Pc^{-2}]$, was formed. Couples IV and V are indicative of metal- and ring-based reductions, respectively, accompanied by the spectral changes, and these changes are presented in Fig. 5b. When the $[Mn^{II}Pc^{-2}]$ is reduced to $[Mn^{I}Pc^{-2}]^{1-}$, the Q band undergoes a hypochromic change, along with the formation of new bands at 474, 509, 605, and 653 nm, and the Q band vanished. When $[Mn^{I}Pc^{-2}]^{1-}$ was reduced to $[Mn^{I}Pc^{-3}]^{2-}$, this caused a hypochromic change in the Q band, and new bands were observed in the MLCT region, which are typical of ring-based reduction behavior in MPcs [25, 46]. During oxidation, Q band was hyperchromic with a tiny bathochromic shift from 745 to 754 nm (Fig. 5c). This is a clear indication of metal-based oxidation and sheds light on $[Cl^{1-}\text{-}Mn^{III}Pc^{-2}]/[Cl^{1-}\text{-}Mn^{IV}Pc^{-2}]^{1+}$ process. During

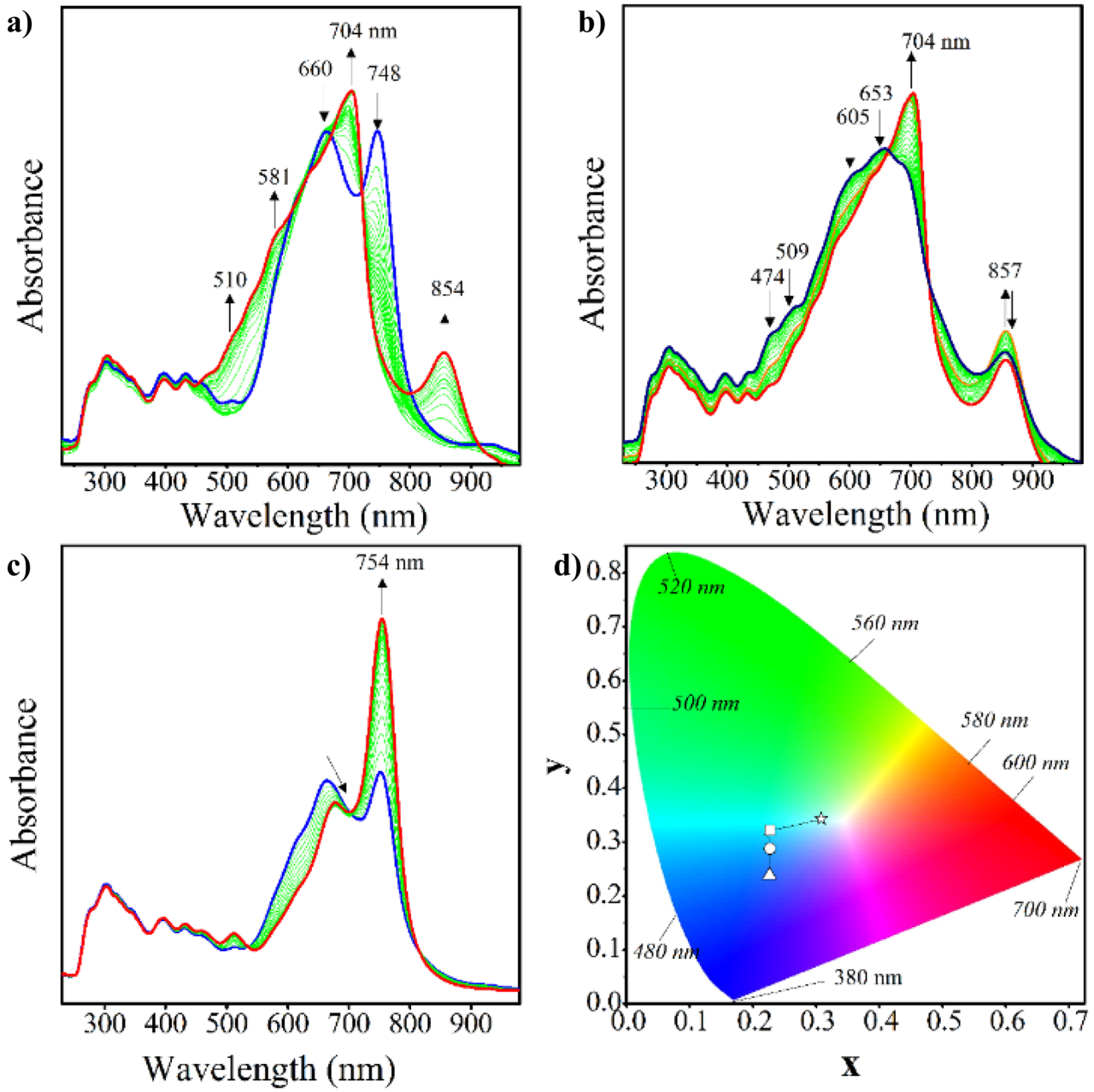

Fig. 5 In situ UV–Vis spectral changes of MnPc in TBAP/DMF electrolyte system. **a)** E_{app} = -0.40 V **b)** E_{appi} = -1.20 V **c)** E_{app} = 1.20 V, **d)** Chromaticity diagram (each symbol represents the color of electro-generated species; □: $[Mn^{III}Pc^{-2}]$; O: $[Mn^{II}Pc^{-2}]^{1-}$; Δ: $[Mn^{II}Pc^{-3}]^{2-}$; ☆: $[Mn^{III}Pc^{-1}]^{1+}$

in situ electrocolorimetry of MnPc, the chromaticity diagram is produced and shown in Fig. 5d. Neutral MnPc is cyan (x = 0.226 and y = 0.322) and it was reduced to blue (x = 0.227 and y = 0.288), and then to dark blue (x = 0.226 and y = 0.238). When neutral MnPc was oxidized, it turned to green (x = 0.308 and y = 0.343).

CV and SWV of FePc, in DMF/TBAP electrolytic system, are presented in Fig. 6. Acetate ion was bound to iron(III) in the neutral state, symbolized as $[Ac^{1-}\text{-}Fe^{III}Pc^{-2}]$. As soon as the circuit is complete, the iron(III) ion was immediately reduced to iron(II), forming the $[Ac^{1-}\text{-}Fe^{II}Pc^{-2}]^{1-}$ species. The redox couple at 0.26 V was ascribed to the reduction process, shown as $[Ac^{1-}\text{-}Fe^{III}Pc^{-2}]$ to $[Ac^{1-}\text{-}Fe^{II}Pc^{-2}]^{1-}$ and at 0.0 V, it was present in the latter form. When scanned anodically with CV and SWV, there were two oxidative processes at 0.56 V (II, $[Ac^{1-}\text{-}Fe^{III}Pc^{-2}]$ / $[Ac^{1-}\text{-}Fe^{III}Pc^{1-}]^{1+}$) and at 1.16 V (I; $[Ac^{1-}\text{-}Fe^{III}Pc^{1-}]^{1+}$ / $[Ac^{1-}\text{-}Fe^{III}Pc^{0}]^{2+}$). $[Ac^{1-}\text{-}Fe^{II}Pc^{-2}]^{1-}$ species reduced to

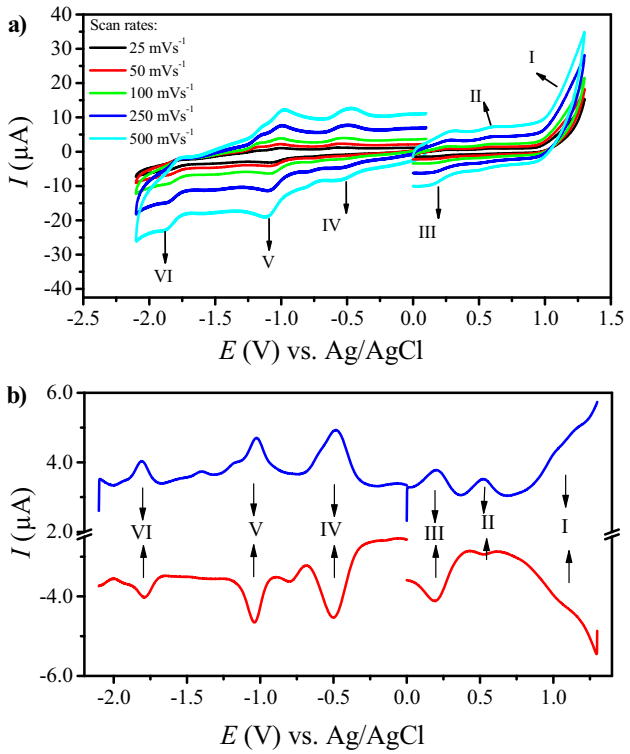

Fig. 6 **a)** CVs of FePc (5.0×10^{-4} mol.dm^{-3}) recorded from 25 to 500 mV/s scan rates and **b)** SWV of FePc recorded at 0.100 Vs^{-1} scan rate on a GCE working electrode in TBAP/DMF electrolyte system

$[Ac^{1-}\text{-}Fe^{I}Pc^{-2}]^{2-}$ at -0.54 V (IV) during cathodic potential scans. The oxidation state of FePc was reduced, and the axial ligand, acetate, was released after the process IV, yielding the $[Fe^{I}Pc^{2-}]^{1-}$ species. There were further reductions, at -1.04 (couple V) and -1.85 V (couple VI), assignable to $[Fe^{I}Pc^{-2}]^{1-}/[Fe^{I}Pc^{-3}]^{2-}$ and $[Fe^{I}Pc^{-3}]^{2-}/[Fe^{I}Pc^{-4}]^{3-}$ processes.

Spectroelectrochemical responses of FePc are also evaluated to provide an exact explanation to the system. The spectral changes of FePc are illustrated in Fig. 7.

When the circuit is established, $[Ac^{1-}\text{-}Fe^{III}Pc^{-2}]$ species were reduced to $[Ac^{1-}\text{-}Fe^{II}Pc^{-2}]^{1-}$ species and thus the spectrum observed at 0.0 V represents response of $[Ac^{1-}\text{-}Fe^{II}Pc^{-2}]^{1-}$ species. Potential applied at -0.70 V led to a hyperchromic change of $[Ac^{1-}\text{-}Fe^{II}Pc^{-2}]^{1-}$ and new peaks emerge at 576 and 810 nm. This is a clear indication of the reduction in $[Ac^{1-}\text{-}Fe^{II}Pc^{-2}]^{1-}$ to $[Ac^{1-}\text{-}Fe^{I}Pc^{-2}]^{2-}$ species (Fig. 7a). Figure 7a shows that, toward the end of the reductive process, the spectral response started to change. The release of acetate ion is eminent in the shift of 810 nm band and hypochromism of the 389 nm band. During this reduction, acetate ion was released from $[Ac^{1-}\text{-}Fe^{I}Pc^{-2}]^{2-}$ and turned to $[Fe^{I}Pc^{-2}]^{1-}$ species. At -1.20 V, the spectral changes pointed to a ring-based reductive change, which can be ascribed to $[Fe^{I}Pc^{-2}]^{1-}$ to $[Fe^{I}Pc^{-3}]^{2-}$ reduction (Fig. 7b). Figure 7c shows the spectral changes during oxidation. Under 0.40 V potential applied, $[Ac^{1-}\text{-}Fe^{II}Pc^{-2}]^{1-}$ species were oxidized to neutral $[Ac^{1-}\text{-}Fe^{III}Pc^{-2}]$. A bathochromic shift of the Q band from 676 to 730 nm is a supportive finding to the oxidation to neutral $[Ac^{1-}\text{-}Fe^{III}Pc^{-2}]$ (Fig. 7c). The hypochromic change of the Q band with the potential application at 0.70 V is an attributable observation to the oxidation of neutral $[Ac^{1-}\text{-}Fe^{III}Pc^{-2}]$ (Fig. 7c inset). In situ colorimetry was exercised in the recording of FePc's redox processes accompanied by color change of the solution (Fig. 7d). When no potential is applied, the solution containing $[Ac^{1-}\text{-}Fe^{II}Pc^{-2}]^{1-}$ species was greenish blue (x = 0.261 and y = 0.362). When the potential was applied by stepping from 0 to -1.20 V, the initial color changed to light blue (x = 0.261 and y = 0.287) and then to blue (x = 0.246 and y = 0.228). The first oxidation led to a color change to turquoise (x = 0.273 and y = 0.348). Between redox species, distinct changes of colors are a consideration of possible use of them in electrochromism.

Electrode modification and oxygen evolution reaction

Our previous paper indicated that MPcs having thiazole groups could be electropolymerized on the electrode surface, thus possibility of the electropolymerizations of MPcs was examined [26]. Metallophthalocyanines with thiazole groups are, as reported by our group, capable of being electropolymerized and thus, we searched the possibility of electropolymerizations of MPcs. It is known that thiazole-containing compounds are easy to electropolymerize in dichloromethane. MPcs having tetrakis [4-(4-methoxyphenyl)-2-thiazole-2-thio] substituents were electropolymerized on the working electrode in DCM/TBAP electrolyte. Repetitive cyclic voltammetry is reported in the literature as a potential electropolymerization technique, which is adopted by us [50–52]. We observed that all compounds were electropolymerized on the working electrode with similar repetitive CV scans. Figure 8 is an example of the electropolymerization of FePc. FePc had two oxidative waves at 1.00 and 1.62 V along with a single reductive wave at 0.31 V. During the first CV, cationic radicals of thiazole groups are formed. These cationic radicals dimerize from the neighboring carbon of the S in the thiazole ring, which is followed by the formation of a sigma bond between two thiazole groups. During the consecutive CV cycles, new nucleation and oligomerization processes are taken place to form conductive MPc film on the electrode surface [53]. The formation of electropolymerized film was evidenced by a cathodic shift during repetitive CVs. The increase in current starts to decrease after the sixth cycle, owing to the decrease in conductivity of the film that is

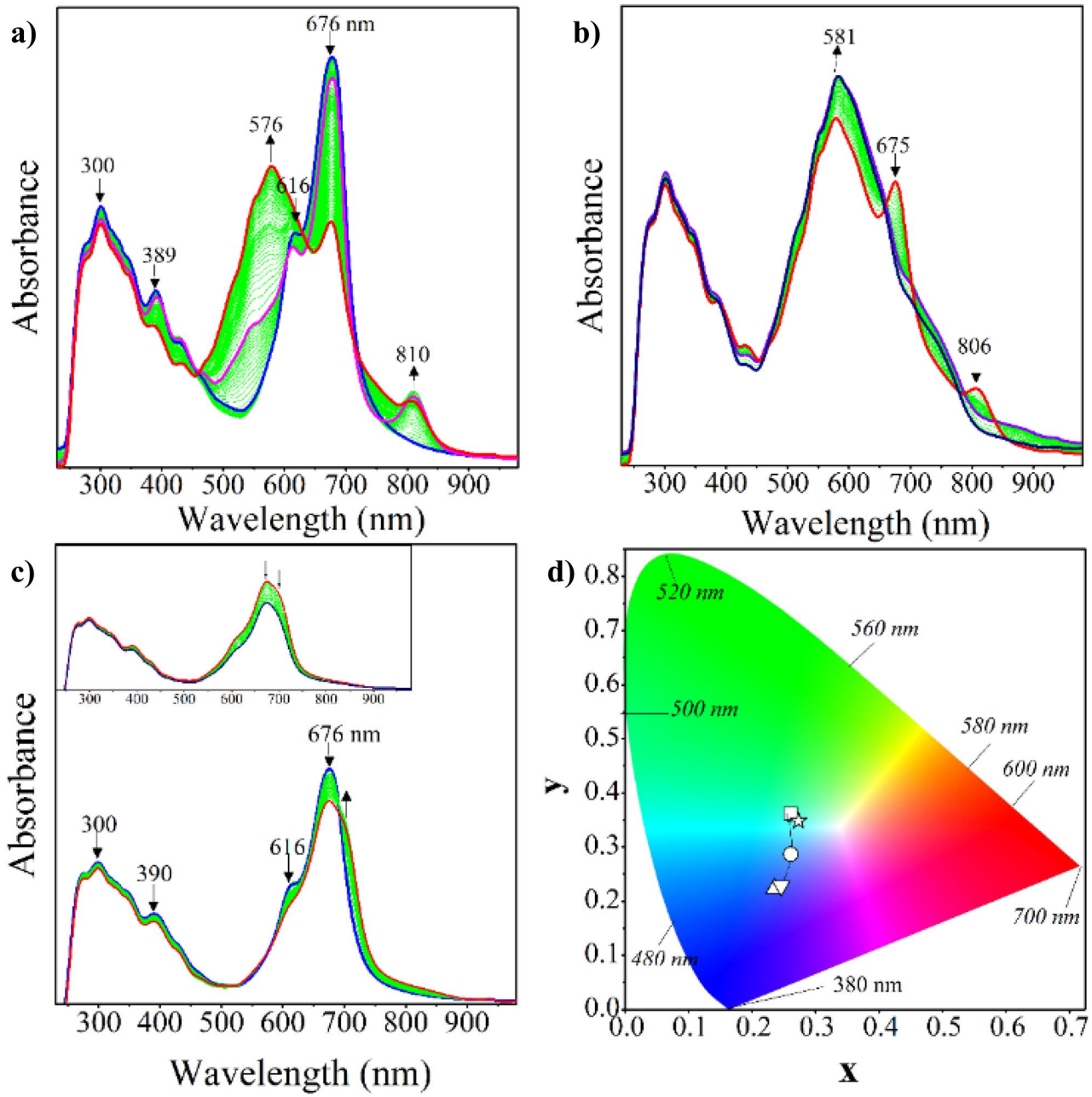

Fig. 7 **a)** E_{app} = -0.70 V **b)** E_{appi} = -1.20 V **c)** E_{app} = 0.40 V (inset; E_{app} = 0.70 V), **d)** Chromaticity diagram (each symbol represents the color of electro-generated species; □: $[Ac^{1-}\text{-}Fe^{II}Pc^{-2}]^{1-}$; O: $[Fe^{I}Pc^{-2}]^{2-}$; Δ: $[Fe^{I}Pc^{-3}]^{3-}$; ☆: $[Ac^{1-}\text{-}Fe^{III}Pc^{-2}]$

formed on the working electrode. GCE/FePc modified electrode is thus optimized after 6 CV cycles.

As a possible electrocatalyst for oxygen evolution reaction (OER), GCE/FePc modified electrocatalyst was tested in 1.0 mol dm^{-3} NaOH electrolyte at the pH of 12.54. For OER catalytic activity, linear sweep voltammetry (LSV) was performed on a rotating disk electrode (RDE) at a 3 mVs^{-1} scan rate within 1.00–2.25 V potential range versus reversible hydrogen electrode (RHE). The experiments were performed versus Ag/AgCl, but the plot was drawn versus RHE46 to compare easily with the literature and to remove the pH effect. In Fig. 9, LSV curves are provided for the fabricated GCE/FePc, commercial GCE/IrO_2, and bare GCE, with onset potentials as 1.57, 1.71, and 1.95 V, respectively. With increased current density, the fabricated GCE/FePc yielded a significantly low onset potential. The fabricated GCE/FePc could be a possible electrocatalyst for the water-splitting reactions.

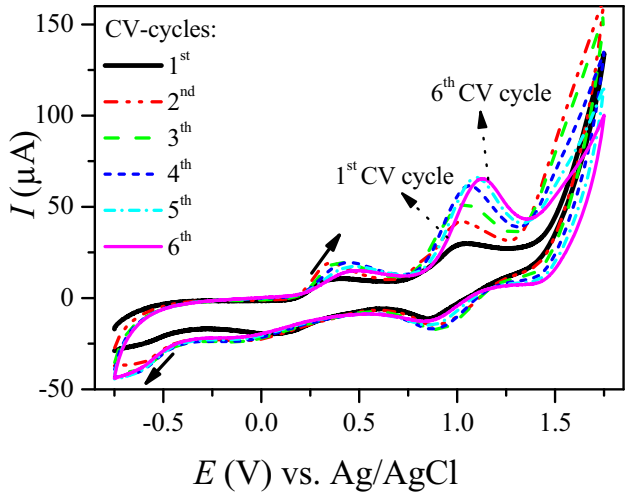

Fig. 8 Electropolymerization of FePc with repetitive CVs in DMF/TBAP electrolyte at 100 mVs^{-1} scan rate

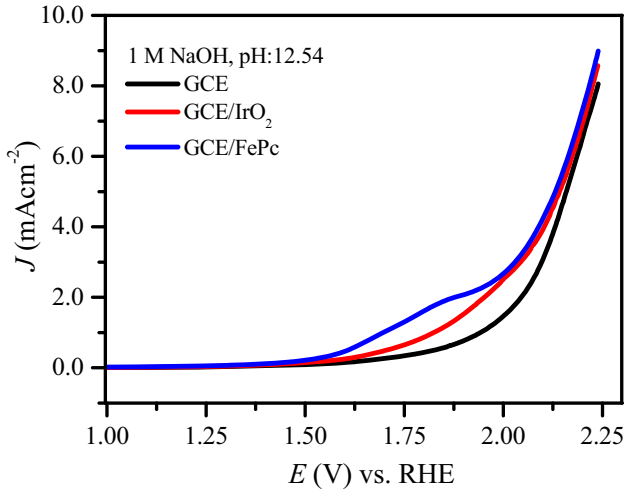

Fig. 9 LSVs on the GCE with a scan rate of 3 mVs^{-1} rotating rate at 600 rpm in 1.00 M NaOH electrolyte (pH: 12.54)

Conclusions

In this work, 4-(4-methoxyphenyl)-2-thiazole-2-thio substitutions at non-peripheral metallophthalocyanines were formed, then ^{1}H-NMR, FT-IR, UV–Vis, and MS data were acquired to characterize the synthesized compounds. The effects of redox-active cobalt (II), chloromanganese (III), and acetatoiron (III) metal centers on electrochemical and spectroelectrochemical properties of the metallophthalocyanines were investigated. Through electrochemical and spectroelectrochemical measurements, the proposed structures of the compounds were suggested. Voltammetric and spectroelectrochemical studies provided the insight that CoPc, MnPc, and FePc underwent metal- and ligand-based, diffusion-controlled, multi-electron and reversible/quasi-reversible redox processes. The presence of multi-electronic metal- and ring-based redox chemistry increases the benefit of the complexes, as functional materials in electrosensing, electrochromisms, and electrocatalysis, being some examples to possible electrochemical applications. In addition, GCE/FePc modified electrode can be operated as an active electrocatalyst for OER, in some examples like PEM and alkaline water electrolysis devices.

Supplementary information The online version contains supplementary material available at https://doi.org/10.1007/s10008-022-05120-2.

Acknowledgements Atıf Koca thanks Turkish Academy of Sciences (TUBA) for support.

Declarations

Conflict of interest The authors declare no competing interests.

References

1. Leznoff CC (1989) Phthalocyanines. Properties and Applications. Wiley-VCH, New York
2. Beduoğlu A, Sevim AM, Koca A, Altındal A, Bayır ZA (2020) Thiazole-substituted non-symmetrical metallophthalocyanines: synthesis, characterization, electrochemical and heavy metal ion sensing properties. New J Chem 44:5201–5210
3. Odabaş Z, Altindal A, Özkaya AR, Salih B, Bekaroğlu Ö (2010) Novel ball-type homo-and hetero-dinuclear phthalocyanines with four 1, 1′-methylenedinaphthalen-2-ol bridges: synthesis and characterization, electrical and gas sensing properties and electrocatalytic performance towards oxygen reduction. Sens Actuators B Chem 145:355–366
4. Kobayashi N, Furuyama T, Satoh K (2011) Rationally Designed Phthalocyanines Having Their Main Absorption Band beyond 1000 nm. J Am Chem Soc 133:19642–19645
5. Bottari G, de la Torre G, Guldi DM, Torres T (2010) Covalent and Noncovalent Phthalocyanine−Carbon Nanostructure Systems: Synthesis, Photoinduced Electron Transfer, and Application to Molecular Photovoltaics. Chem Rev 110:6768–6816
6. Alzate-Carvajal N, Bolivar-Pineda LM, Meza-Laguna V, Basiuk VA, Basiuk EV, Baranova EA (2020) Oxygen Evolution Reaction on Single-Walled Carbon Nanotubes Noncovalently Functionalized with Metal Phthalocyanines. ChemElectroChem 7:428–436
7. Agboola B, Nyokong T (2007) Comparative electrooxidation of nitrite by electrodeposited Co(II), Fe(II) and Mn(III) tetrakis (benzylmercapto) and tetrakis (dodecylmercapto) phthalocyanines on gold electrodes. Anal Chim Acta 587:116–123
8. Aydemir M, Karaoğlu HRP, Koçak MB, Koca A (2015) Immobilization of alkynyl functionalized manganese phthalocyanine via click electrochemistry for electrocatalytic oxygen evolution reaction. J Electrochem Soc 162:H170–H178
9. Demirbaş Ü, Akyüz D, Akcay HT, Koca A, Mentese E, Kantekin H (2018) Novel 1, 2, 4-triazole substituted metallophthalocyanines: Synthesis, characterization and investigation of electrochemical and spectroelectrochemical properties. J Mol Struct 1173:205–212

10. Somani PR, Radhakrishnan S (2003) Electrochromic materials and devices: present and future. Mater Chem Phys 77:117–133
11. Domínguez C, Pérez-Alonso FJ, Salam MA, De La Fuente JLG (2014) Effect of transition metal (M: Fe, Co or Mn) for the oxygen reduction reaction with non-precious metal catalysts in acid medium. Int J Hydrog Energy 39:5309–5318
12. Akyüz D, Dinçer H, Özkaya AR, Koca A (2015) Electrocatalytic hydrogen evolution reaction with metallophthalocyanines modified with click electrochemistry. Int J Hydrog Energy 40:12973–12984
13. Dalkılıç Z, Lee CB, Choi H, Nar I, Yavuz NK, Burat AK (2020) Tetra and octa substituted Zn(II) and Cu(II) phthalocyanines: Synthesis, characterization and investigation as hole-transporting materials for inverted type-perovskite solar cells. J Organomet Chem 922:121419
14. Kadish KM, Smith KM, Guilard R (2003) The porphyrin handbook. Academic Press, San Diego
15. Aralekallua S, Sajjana VA, Palanna M, Prabhu KCP, Hojamberdiev M, Sannegowda LK (2020) Ni foam-supported azo linkage cobalt phthalocyanine as an efficient electrocatalyst for oxygen evolution reaction. J Power Sources 449:227516
16. Liao Z, Wang Y, Wang Q, Cheng Y, Xiang Z (2019) Bimetal-phthalocyanine based covalent organic polymers for highly efficient oxygen electrode. Appl Catal B 243:204–211
17. Zhang C, Hao R, Yin H, Liua F, Hou Y (2012) Iron phthalocyanine and nitrogen-doped graphene composite as a novel non-precious catalyst for the oxygen reduction reaction. Nanoscale 4:7326–7329
18. Jiang Y, Lu Y, Lv X, Han D, Zhang Q, Niu L, Chen W (2013) Enhanced Catalytic Performance of Pt-Free Iron Phthalocyanine by Graphene Support for Efficient Oxygen Reduction Reaction. ACS Catal 3:1263–1271
19. Yang J, Tao J, Isomura T, Yanagi H, Moriguchi I, Nakashima N (2019) A comparative study of iron phthalocyanine electrocatalysts supported on different nanocarbons for oxygen reduction reaction. Carbon 145:565–571
20. Chen K, Liu K, An P, Li H, Lin Y, Hu J, Jia C, Fu J, Li H, Liu H, Lin Z, Li W, Li J, Lu Y-R, Chan T-S, Zhang N, Liu M (2020) Iron phthalocyanine with coordination induced electronic localization to boost oxygen reduction reaction. Nat Commun 11:4173
21. Dede G, Bayrak R, Er M, Özkaya AR, Değirmencioğlu İ (2013) DBU-catalyzed condensation of metal free and metallophthalocyanines containing thiazole and azine moieties: Synthesis, characterization and electrochemical properties. J Organomet Chem 740:70–77
22. Demirbaş Ü, Akçay HT, Koca A, Kantekin H (2017) Synthesis, characterization and investigation of electrochemical and spectroelectrochemical properties of peripherally tetra 4-phenylthiazole-2-thiol substituted metal-free, zinc (II), copper (II) and cobalt (II) phthalocyanines. J Mol Struct 1141:643–649
23. Nečedová M, Magdolen P, Novakova V, Cigáň M, Vlčková S, Zahradník P, Fülöpová A (2015) Synthesis and Photophysical, Electrochemical and Theoretical Study of Thiazole-Annelated Phthalocyanine. Eur J Org Chem 2015:7053–7068
24. Duruk EG, Yenilmez HY, Koca A, Bayır ZA (2015) Synthesis, electrochemical and spectroelectrochemical properties of thiazole-substituted phthalocyanines. Synth Met 209:361–368
25. Uzunmehmetoğlu HZ, Yenilmez HY, Kaya K, Koca A, Altındal A, Bayır ZA (2007) Electrochemical, spectroelectrochemical, and dielectric properties of metallophthalocyanines bearing redox active cobalt and manganese metal centres. Inorganica Chim Acta 459:51–62
26. Demir F, Yenilmez HY, Koca A, Bayır ZA (2019) Metallophthalocyanines containing thiazole moieties: Synthesis, characterization, electrochemical and spectroelectrochemical properties and sensor applications. J Electroanal Chem 832:254–265
27. Nar I, Atsay A, Altındal A, Hamuryudan E, Koçak MB, Gül A (2018) Ferrocenyl Phthalocyanine as Donor in Non-Poly(3-hexylthiophen-2,5-diyl) Bulk Heterojunction Solar Cell. Chem - A Eur J 24:6946–6949
28. Çelik Ç, Farajzadeh N, Akın M, Atmaca GY, Sağlam Ö, Şaki N, Erdoğmuş A, Koçak MB (2021) Investigation of the biological and photophysicochemical properties of new non-peripheral fluorinated phthalocyanines. Dalton Trans 50:2736–2745
29. Ghani F, Kristen J, Riegler H (2012) Solubility Properties of Unsubstituted Metal Phthalocyanines in Different Types of Solvents. J Chem Eng Data 57:439–449
30. Schaffer AM, Gouterman M, Davidson ER (1973) XXVIII. Extended hückel calculations on metal phthalocyanines and tetrazaporphins. Theor Chim Acta 30:9–30
31. Isago H (2015) Optical Spectra of Phthalocyanines and Related Compounds. Springer Japan, Japan
32. Bayır Z (2005) Synthesis and characterization of novel soluble octa-cationic phthalocyanines. Dyes Pigm 65:235–242
33. Mack J, Stillman M (2001) Assignment of the optical spectra of metal phthalocyanines through spectral band deconvolution analysis and ZINDO calculations. Coord Chem Rev 219–221993–1032
34. Koçan H, Burat AK (2013) Synthesis and characterization of [7-(trifluoromethyl)- quinolin-4-yl]oxy-substituted phthalocyanines. Mon Chem 144:171–177
35. Değirmencioğlu İ, Er M, Bayrak R, Özkaya AR (2017) Redox-Switchable New Phthalocyanines Containing Hydrazono-Thiazole-Carboxylate Fragments: Synthesis, Electrochemical, Spectroelectrochemical and Electrocolorimetric Investigation. J Fluoresc 27:869–881
36. Yenilmez HY, Akdağ Ö, Aytuğ MS, Koca A, Bayır ZA (2015) Electrochemical, spectroelectrochemical characterization and electropolymerization of 2-(4-methyl-1, 3-thiazol-5-yl) ethoxy-substituted manganese and indium phthalocyanines. Polyhedron 99:244–251
37. Lukyanets EA, Nemykin VN (2010) The key role of peripheral substituents in the chemistry of phthalocyanines and their analogs. J Porphyr Phthalocyanines 14:1–40
38. Kobayashi N, Ogata H, Nonaka N, Luk'yanets EA (2003) Effect of Peripheral Substitution on the Electronic Absorption and Fluorescence Spectra of Metal-Free and Zinc Phthalocyanines. Chem Eur J 9:5123–5134
39. Akinbulu IA, Nyokong T (2010) Syntheses and investigation of the effects of position and nature of substituent on the spectral, electrochemical and spectroelectrochemical properties of new cobalt phthalocyanine complexes. Polyhedron 29:1257–1270
40. Ough E, Nyokong T, Creber KAM, Stillman MJ (1989) Phthalocyanines: properties and applications. VCH, New York, p 139
41. de A. Soares II L, Trsic M, Berno B, Aroca R, (1996) Electronic spectra of metal phthalocyanines and configuration interaction ZINDO calculations for tetra-azaporphyrin complexes with the first transition metal series. Spectrochim Acta A10:1245–1253
42. Sakamoto K, Ohno-Okumura E (2009) Syntheses and functional properties of phthalocyanines. Materials 2:1127–1179
43. Arıcı M, Arıcan D, Uğur UL, Erdoğmuş A, Koca A (2013) Electrochemical and spectroelectrochemical characterization of newly synthesized manganese, cobalt, iron and copper phthalocyanines. Electrochim Acta 87:554–566
44. Ozoemena KI, Nyokong T (2006) Comparative electrochemistry and electrocatalytic activities of cobalt, iron and manganese phthalocyanine complexes axially co-ordinated to mercaptopyridine self-assembled monolayer at gold electrodes. Electrochim Acta 51:2669–2677
45. Dzieciuch MA, Gupta N, Wroblowa HS (1988) Rechargeable Cells with Modified MnO_2 Cathodes. J Electrochem Soc 135:2415–2419

46. Simic-Glavaski B, Tanaka AA, Kenney ME, Yeager E (1987) Spectroscopic and electrochemical studies of transition-metal tetrasulfonated phthalocyanines: Part VIII. Spectroelectrochemical studies of stacked-ring silicon phthalocyanines. J Electroanal Chem Interfacial Electrochem 229:285–296
47. Zecevic S, Simic-Glavaski B, Yeagear E, Lever ABP, Minor PC (1985) Spectroscopic and electrochemical studies of transition metal tetrasulfonated phthalocyanines: Part V. Voltammetric studies of adsorbed tetrasulfonated phthalocyanines (MTsPc) in aqueous solutions. J Electroanal Chem Interfacial Electrochem 196:339–358
48. Garip EÖ, Özçeşmeci M, Nar I, Özçeşmeci İ, Hamuryudan E (2018) Novel phthalocyanines containing azo chromophores; synthesis, characterization, photophysical, and electrochemical properties. J Porphyr Phthalocyanines 22:198–206
49. Göktuğ Ö, Akyüz D, Koca A, Şener MK (2017) Synthesis and electropolymerization of EDOT modified 1, 3-bis (5-methyl-2-thiazolylimino) isoindolinato palladium (II) complex for electrochemical detection of hydrogen peroxide. J Coord Chem 70.2052–2060
50. Kobak RZU, Akyüz D, Koca A (2016) Substituent effects to the electrochromic behaviors of electropolymerized metallophthalocyanine thin films. J Solid State Electr 20:1311–1321
51. Akyüz D, Keles T, Bıyıklıoğlu Z, Koca A (2017) Electrochemical pesticide sensors based on electropolymerized metallophthalocyanines. J Electroanal Chem 804:53–63
52. Wang L, Lee CY, Schmuki P (2013) Solar water splitting: preserving the beneficial small feature size in porous α-Fe_2O_3 photoelectrodes during annealing. J Mater Chem A 1:212–215
53. Heinze J, Frontana-Uribe BA, Ludwigs S (2010) Electrochemistry of Conducting Polymers—Persistent Models and New Concepts. Chem Rev 110:4724–4771